L04

Proceedings of the 5th International Conference on Inverse Problems in Engineering: Theory and Practice, Cambridge, UK, 11-15th July 2005

COMPARISON OF TWO INVERSE SCATTERING ALGORITHMS FOR THE EXPERIMENTAL SYNTHESIS OF FIBER BRAGG GRATINGS

D. LEDUC[1], X. CHAPELEAU[1], C. LUPI[1], F. LOPEZ GEJO[2], M. DOUAY[2], R. LE NY[1] and C. BOISROBERT[1]

[1]*IREENA, Faculté des Sciences et des Techniques de Nantes, 2 rue de la houssinière, 44322 Nantes, France*
[2]*PhLAM, Université des Sciences et Technologies de Lille, 59655 Villeneuves d'Ascq, France*
e-mail: dominique.leduc@physique.univ-nantes.fr

Abstract- In this paper we use inverse scattering algorithms to synthesize the index profiles of Fibre Bragg Gratings from Low Coherence Interferometry measurements. We compare two algorithms : the Layer Peeling and an iterative solution of the Gel'fand-Levitan-Marchenko coupled equations and show that the former is more efficient.

1. INTRODUCTION

Fibre Bragg Gratings (FBG) are usually made by irradiating an optical fibre with UV light to periodically modulate the refractive index of the fibre core. These components behave as filters : they reflect a narrow spectral band of the incoming light. The reflection coefficient of a grating depends on its length and its index modulation amplitude. The central wavelength depends on the grating period. Fibre Bragg Gratings find wide applications in optical telecommunication networks (gain flattening, multiplexing/demultiplexing, chromatic dispersion compensation) and in the field of sensors.

Accurate determination of the index profile of FBG is essential but very difficult to achieve with direct measurements. Inverse methods can be used, but they require to measure the *complex* reflection coefficient of the grating. This has prevented a long time their use for real FBG. The main part of the research in this field was devoted to the design of gratings, *ie* the determination of index profile of the grating whose spectral properties correspond to target functions. But, it has been recently demonstrated that Low Coherence Interferometry (LCI) can accurately measure the complex reflection coefficient of FBG, [3, 8]. This makes possible the reconstruction of real gratings with an appropriate synthesis algorithm. Such reconstruction using the "Layer-Peeling" (LP) algorithm have already been reported, [2, 5]. This algorithm was chosen because it seemed to be the most powerful but others methods exist such as the iterative solution of the Gel'fand-Levitan-Marchenko coupled equations (GLM). In order to perform a deeper study of gratings synthesis, we implemented both LP and GLM algorithms. In this paper we present these algorithms and compare their efficiencies.

2. DESCRIPTION OF THE ALGORITHMS

2.1 Coupled modes theory

Both algorithms are based on the coupled modes theory, [7, 17]. In the scalar approximation, the electrical field inside the fibre obeys the wave eqn. :

$$\nabla^2 E(x,y,z,t) = \frac{n^2(x,y,z)}{c^2}\frac{\partial^2}{\partial t^2}E(x,y,z,t) \tag{1}$$

where $n(x,y,z)$ is the refractive index, (x,y) are the transverse co-ordinates and z the longitudinal co-ordinate. The fibre is assumed to be lossless and single-mode. It implies that two contrapropagative waves propagates inside it :

$$E(x,y,z,t) = \Psi(x,y)\left[e^{-i(\omega t-\beta z)} + e^{-i(\omega t+\beta z)}\right] \tag{2}$$

where β is the propagation constant and $\Psi(x,y)$ the propagating mode with an overlap factor η. From eqn. (1) we obtain :

$$\left[\frac{\partial^2}{\partial x^2}+\frac{\partial^2}{\partial y^2}-\left(\beta^2-\frac{n_{\text{eff}}^2(x,y)\,\omega^2}{c^2}\right)\right]\Psi(x,y) = 0 \tag{3}$$

Inside the grating, the refractive index is periodically modulated along the longitudinal axe. We have then $n(x,y,z) = n_{\text{eff}}(x,y) + \Delta n(z)$, with

$$\Delta n(z) = \Delta n_{\text{DC}}(z) + \Delta n_{\text{AC}}(z)\ \cos\left[\frac{2\pi}{\Lambda_0}z + \frac{2\pi}{\Lambda_0^2}\int_0^z (\Lambda(z')-\Lambda_0)\,dz'\right] \tag{4}$$

where $\Delta n_{AC}(z)$ is the index modulation amplitude, $\Delta n_{DC}(z)$ the average effective index, $\Lambda(z)$ the local period of modulation and $\Lambda_0 = \Lambda(0)$. We then have to assume that the forward and backward waves have envelopes $u_f(z)$ and $u_b(z)$. The electrical field becomes :

$$E(x,y,z,t) = \Psi(x,y)\left\{u_f(z)\,e^{-i[\omega t-(\beta-\delta)z-\psi_{DC}]} + u_b(z)\,e^{-i[\omega t+(\beta-\delta)z+\psi_{DC}(z)]}\right\} \tag{5}$$

where $\delta = \beta - \pi/\Lambda_0$ and $\psi_{DC}(z) = (\eta\pi/n_{eff}\Lambda_0)\int_0^z \Delta n_{DC}(z')\mathrm{d}z'$. We insert this expression in the wave eqn. (1) and integrate in the transverse plane to remove the transverse dependency with the help of eqn. (3). Neglecting the rapidly oscillating terms [12], we obtain :

$$\begin{pmatrix} i\partial_z & \Omega(z) \\ \Omega^*(z) & -i\partial_z \end{pmatrix}\begin{pmatrix} u_f(z) \\ u_b(z) \end{pmatrix} = -\delta \begin{pmatrix} u_f(z) \\ u_b(z) \end{pmatrix} \tag{6}$$

where

$$\Omega(z) = \frac{K}{2}\Delta n_{AC}(z)\,\exp\left[-2i\left(K\int_0^z \Delta n_{DC}(z\prime)\,dz\prime + \frac{\pi}{\Lambda_0^2}\int_0^z (\Lambda(z\prime)-\Lambda_0)\,dz\prime\right)\right] \tag{7}$$

with $K = \eta\pi/n_{eff}\Lambda_0$. We can see that the forward and backward waves are coupled by the grating via the coupling coefficient $\Omega(z)$.

2.2 GLM algorithm

We will outline the most remarkable features of the algorithm, more detailed descriptions can be found in [1, 14, 16]. The grating coupling coefficient is necessarily vanishing outside the grating : $\lim_{z\to\pm\infty}\Omega(z) = 0$. Solutions of eqn. (6) must then behave as $\exp(\pm i\delta z)$ or 0 in the limit as $z \to \pm\infty$. We introduce the Jost functions ϕ, $\bar{\phi}$, ψ and $\bar{\psi}$, solutions of eqn. (6) with boundary conditions :

$$\begin{aligned} \lim_{z\to+\infty}\psi(z,\delta)\exp[-i\delta z] &= \lim_{z\to-\infty}\bar{\phi}(z,\delta)\exp[-i\delta z] = \begin{pmatrix} 1 \\ 0 \end{pmatrix} \\ \lim_{z\to\infty}\bar{\psi}(z,\delta)\exp[i\delta z] &= \lim_{z\to-\infty}\phi(z,\delta)\exp[i\delta z] = \begin{pmatrix} 0 \\ 1 \end{pmatrix} \end{aligned} \tag{8}$$

Then $\phi(z,\delta) = [\phi_1(z,\delta),\phi_2(z,\delta)]^T$ implies $\bar{\phi}(z,\delta) = [\phi_2^*(z,\delta),\phi_1^*(z,\delta)]^T$. The superscript "T" denotes the transpose and the superscript "$*$" the complex conjugate. Since the ψ and $\bar{\psi}$ are linearly independent, we may write : $\bar{\psi}(z,\delta) = a(\delta)\,\bar{\phi}(z,\delta) + b(\delta)\,\phi(z,\delta)$. If we divide this equation by $a(\delta)$, we obtain :

$$\frac{\bar{\psi}(z,\delta)}{a(\delta)} = \bar{\phi}(z,\delta) + \frac{b(\delta)}{a(\delta)}\,\phi(z,\delta) \tag{9}$$

According to eqn. (8), $b(\delta)/a(\delta)$ is associated to the reflection coefficient $r(\delta)$, [1]. Assuming the following integral representation for $\bar{\phi}$:

$$\bar{\phi}(z,\delta) = \begin{pmatrix} 1 \\ 0 \end{pmatrix}\exp[i\delta z] + \int_{-\infty}^{z} A(z,\tau)\exp[i\delta\tau]\,\mathrm{d}\tau \tag{10}$$

eqn. (9) becomes

$$\frac{\bar{\psi}(z,\delta)}{a(\delta)} = \begin{pmatrix} 1 \\ 0 \end{pmatrix}\exp[i\delta z] + \int_{-\infty}^{z}\begin{pmatrix} A_1(z,\tau) \\ A_2(z,\tau) \end{pmatrix}\exp[i\delta\tau]\mathrm{d}\tau + \begin{pmatrix} 0 \\ 1 \end{pmatrix} r(\delta)\exp[-i\delta z] + \int_{-\infty}^{z}\begin{pmatrix} A_2^*(z,\tau) \\ A_1^*(z,\tau) \end{pmatrix}\exp[-i\delta\tau]\mathrm{d}\tau \tag{11}$$

We operate on this equation with $\int_{-\infty}^{+\infty}\exp[-i\delta y]\mathrm{d}y$, interchange integrals, and obtain :

$$\begin{pmatrix} A_1(z,y) \\ A_2(z,y) \end{pmatrix} + \begin{pmatrix} 1 \\ 0 \end{pmatrix}F(z+y) + \int_{-\infty}^{z}\begin{pmatrix} A_2^*(z,\tau) \\ A_1^*(z,\tau) \end{pmatrix}F(\tau+y)\,\mathrm{d}\tau = 0 \tag{12}$$

where $F(z)$ is the Fourier transform of the complex reflection coefficient :

$$F(z) = \int_{-\infty}^{+\infty} r(\delta)\,\mathrm{e}^{-i\delta z}\,\mathrm{d}\delta \tag{13}$$

By substituting the integral representation (10) into eqn. (6), after an integration by parts, one obtains, [1] :

$$\Omega(z) = -2A_1(z,z) \tag{14}$$

So we have to determine $A_1(z,\tau)$ to characterise the grating. Analytical solutions exist when the reflection coefficient is a rational function [15], but for real gratings it is better to use an iterative procedure, [9].

At first order the multiple reflections inside the gratings are neglected : $A_1(z,y) = -F(z+y)$ and the coupling coefficient is approximated by :

$$\Omega_0(z) = -2F(2z) \tag{15}$$

which corresponds to the Born approximation. This solution is inserted in eqn. (12). This gives the first order approximation for A_2 :

$$A_2(z,y) = \int_{-\infty}^{z} F^*(z+\tau)\, F(\tau+y)\, \mathrm{d}\tau \tag{16}$$

which in turn leads to the second order approximation of A_1 :

$$A_1(z,y) = -F(z+y) - \int_{-\infty}^{z}\int_{-\infty}^{z} F(z+u)\, F^*(u+\tau)\, F(\tau+y)\, \mathrm{d}u\, \mathrm{d}\tau \tag{17}$$

then

$$\Omega_1(z) = -2F(2z) - 2\int_{-\infty}^{2z}\int_{-\infty}^{x_1} F(x_2 - x_1 + 2z)\, F^*(x_2)\, F(x_1)\, \mathrm{d}x_2\, \mathrm{d}x_1 \tag{18}$$

This procedure can be repeated several times to get more accurate determination of the coupling coefficient. The general solution has the form :

$$\Omega_p(z) = -2F(2z) - \sum_{m=0}^{p} X_{2m+1}(z,z) \tag{19}$$

where

$$\begin{cases} X_{2m}(z,t) &= \displaystyle\int_{-\infty}^{t} F^*(x)\, X_{2m-1}(z, x-t+2z)\, \mathrm{d}x \\ X_{2m+1}(z,t) &= \displaystyle\int_{-\infty}^{t} F(x)\, X_{2m}^*(z, x-t+2z)\, \mathrm{d}x \end{cases} \tag{20}$$

2.3 Layer Peeling algorithm

This method was at first implemented to solve problems in geophysics [11] and then adapted to the synthesis of FBG, [4, 10, 13]. In this method, the grating is cut out in thin layers with thickness $\Delta\ell$. Each section is supposed to be uniform, the j^{th} section having a modulation amplitude $\Delta n_{\mathrm{AC}}(j\Delta\ell)$ and an average index $\Delta n_{\mathrm{DC}}(j\Delta\ell)$. The Layer Peeling is based on the fact that, at a given moment, the reflected light cannot come from a point in the grating located beyond a certain limit. Thus, initially at t=0, the light can be reflected by the first layer only. This implies that the transfer function $h(0)$ at this moment is proportional to ρ_1, the reflection coefficient of this first section: $h(0) = \rho_1/2\Delta\ell$. However, the transfer function is given by the Fourier transform of the complex reflection coefficient of the grating $r(\delta)$

$$h(z = v\,t) = \frac{1}{2\pi}\int_{-\infty}^{+\infty} r(\delta)\, \mathrm{e}^{-i\delta z}\, \mathrm{d}\,\delta \tag{21}$$

If $\Delta\delta$ is the wavenumber sampling step and M the samples number, one obtains :

$$\rho_1 = 2\Delta\ell\, h(0) = \frac{\Delta\ell\,\Delta\delta}{\pi}\sum_{k=1}^{\mathrm{M}} r(k\,\Delta\delta) \tag{22}$$

The first layer reflection coefficient can then be easily calculated since the complex reflection coefficient of the grating is known. We thus so far have to link ρ_1 to the characteristics of the layer (Δn_{AC}, Δn_{DC} and Λ). In the framework of the coupled modes theory [7, 17], the electric field in the grating is the superposition of the fields of two contrapropagative waves coupled by the grating. A propagation matrix T^j is associated to the layer j. It connects the forward and backward fields at the backplane of the layer to the fields at its frontplane. The reflection coefficient (ρ_j) of this layer is the ratio of the backward and forward fields amplitudes at the frontplane of the layer :

$$\rho_j = -\frac{T_{21}^j}{T_{22}^j} = i\tanh|\Omega(j\Delta\ell)|\, \mathrm{e}^{-i\arg[\Omega(j\Delta\ell)]} \tag{23}$$

where $\Omega(j\Delta\ell)$ is the coupling coefficient of the considered layer. Using eqns (7), (22) and (23), we can determine the characteristics of the first layer from the complex reflection coefficient of the grating. Once the first section is characterised, its transfer matrix is known. It is then possible to propagate the fields through it and calculate the complex reflection coefficient of the grating without its first section. We then find ourselves in the same situation as at the beginning, we can use the same method to characterise the second section and so on until the grating is entirely synthesized.

2.4 Determination of the characteristics of the grating

Once the coupling coefficient $\Omega(z)$ is calculated using eqn. (19) or (23), the determination of the index amplitude modulation is straightforward. eqn. (7) implies :

$$\Delta n_{AC}(z) = \frac{2\, n_{eff}\, \Lambda_0}{\eta\, \pi} \, |\Omega(z)| \tag{24}$$

The determinations of $\Delta n_{DC}(z)$ and $\Lambda(z)$ are more difficult because these two parameters modify the optical path. The variation of the grating phase is a mixture of both influences :

$$\arg[\,\Omega(z)\,] = -\frac{2\pi\,\eta}{n_{eff}\,\Lambda_0} \int_0^z \Delta n_{DC}(z')\, dz' - \frac{2\pi}{\Lambda_0^2} \int_0^z (\Lambda(z') - \Lambda_0)\, dz' \tag{25}$$

It means that one needs *a priori* information to distinguish $\Delta n_{DC}(z)$ from $\Lambda(z)$.

We studied two kind of gratings : uniform and chirped gratings. The period of an uniform grating is constant along the grating ($\Lambda(z) = \Lambda_0$). The phase variation is then only due to the mean effective index. So, eqn. (25) becomes :

$$\Delta n_{DC}(z) = -\frac{n_{eff}\,\Lambda_0}{2\,\pi\,\eta} \frac{d}{dz} (\arg[\,\Omega(z)\,]) \tag{26}$$

The chirped gratings we worked on were written by the phase-mask technique, using a mask with a linear chirp. We then assumed that the period of the grating was varying linearly, $\Lambda(z) = \Lambda_0 + \alpha z$, and that the mean effective index was uniform or oscillated around a mean value, $\Delta n_{DC}(z) = \overline{\Delta n_{DC}} + f(z)$. The rapidly oscillating function $f(z)$ was added to the model because the first uniform gratings we considered exhibited irregularities [2] in $\Delta n_{AC}(z)$ and in $\Delta n_{DC}(z)$. With the previous assumptions, the grating phase given by eqn. (25) becomes :

$$\arg[\,\Omega(z)] = -\frac{2\pi\,\eta\,\overline{\Delta n_{DC}}}{n_{eff}\,\Lambda_0}\, z - \frac{\pi}{\Lambda_0^2}\,\alpha\, z^2 - \frac{2\pi\,\eta}{n_{eff}\,\Lambda_0} \int_0^z f(z')\, dz' \tag{27}$$

Thus, the grating phase oscillates around a parabola. The key point is that the second order coefficient only depends on the chirp. So, when we fit the experimental phase curve by a quadratic function, we can retrieve immediately the chirp parameter α. Once we have done that, the determination of the mean effective index is straightforward since we only need to subtract the function $\pi\alpha z^2/\Lambda_0$ from the grating phase.

3. LOW COHERENCE INTERFEROMETRY

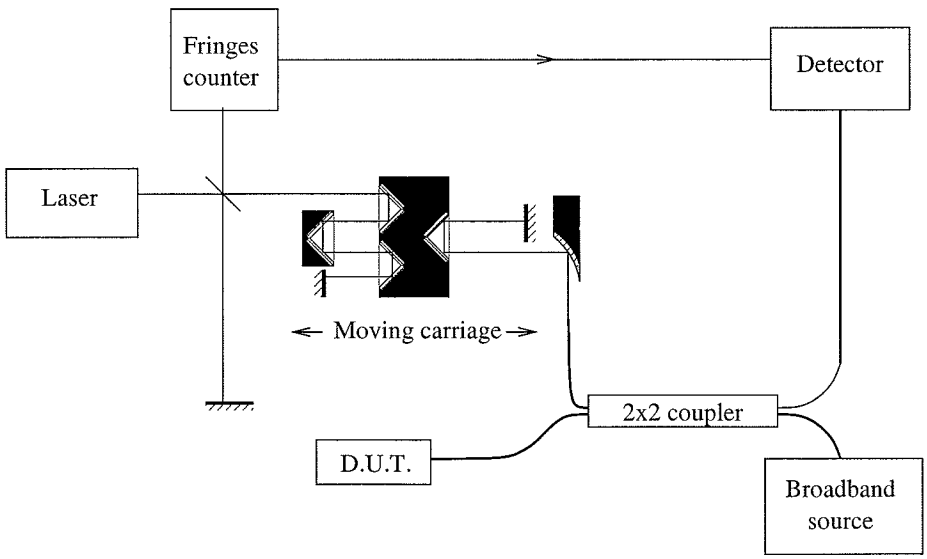

Figure 1: Low coherence interferometer.

Obviously, the accuracy of the grating synthesis using LP or GLM algorithm largely depends on the accuracy with which the complex reflection coefficient is determined. The experimental device that we implemented is shown in Figure 1. It is made of two coupled Michelson interferometers. The first one, in the lower right corner of the figure, uses a broadband infrared light source. The incident light is splitted by a 2×2 fibre coupler. One part is launched in the test arm, where the studied grating is connected, and the other in the reference arm. An airborne

sliding corner cube allows to vary the optical path in the reference arm. The position of the corner cube is accurately measured by the second Michelson interferometer. Its signal is used to sample the infrared interferogram. When the corner-cube carriage slides along the rail, the infrared interferograms are detected by the InGaAs-PIN photoreceiver. The amplitude of the waves coming from the reference and test arms are respectively given by :

$$E_r(t) = \int_{-\infty}^{+\infty} r_r(\sigma)\rho(\sigma)e^{i[2\pi ct - L_r(\sigma)]\sigma}d\sigma \quad \text{and} \quad E_t(t) = \int_{-\infty}^{+\infty} r_t(\sigma)\rho(\sigma)e^{i[2\pi ct - L_t(\sigma)]\sigma}d\sigma \tag{28}$$

where σ is the wavenumber, $\rho(\sigma)$ the spectral density of amplitude of the source, $r_r(\sigma)$ the reflection coefficient of the reference arm and $r_t(\sigma)$ the complex reflection coefficient of the device under test. $L_r(\sigma)$ and $L_t(\sigma)$ are respectively the two-ways optical paths of the reference and test arms.

The recorded signal is equal to $\left\langle |E_r(t) + E_t(t)|^2 \right\rangle_t$, where the brackets denote the temporal average. It is the superposition of a DC signal corresponding to the intensities reflected by each arm and an AC one created by the interference of the two waves. The receiver is AC coupled and amplifies the oscillations only. Using eqn. (28), we find that the variable part of the intensity is [8]:

$$I(z) = \int_{-\infty}^{+\infty} r_t(\sigma)S(\sigma)e^{i\phi(\sigma)}e^{-8i\pi\sigma z}d\sigma \tag{29}$$

where $\phi(\sigma)$ is the phase difference between the interfering waves, $S(\sigma) = r_r(\sigma)|\rho(\sigma)|^2$ the source spectral power density filtered by the system and z the displacement of the moving carriage. The complex reflection of a grating can then easily be calculated from the recorded interferogram, using a Fourier transform.

4. EXPERIMENTAL RESULTS

4.1 Modulation amplitude

The gratings were inscribed, by means of the standard phase mask technique [6], onto standard SMF 28 fibres, previously hydrogenated in order to enhance its photosensitivity. Light of wavelength 248 nm from a pulsed laser source was used to irradiate the fibres. For the inscription of uniform gratings (Unif1, Unif2 and Unif3) and the step grating called Step2, we used a regular phase mask, with period 1071 nm. In the case of the step grating, two steps of length 4 mm each one were written sequentially, one next to the other, by displacing the fibre with respect to the mask. Each step differs from the previous in the total amount of radiation (i.e. number of pulses) received during inscription. In the case of the chirped gratings, we employed two types of phase mask. A first one with linear variation of the period (chirp) 3 nm/cm, central period 1071 nm, and total length of 1 cm, was used to inscribe gratings Chirp2, Chirp3 and Chirp4. A second mask, also linear but with period 0.05 nm/cm was used to produce grating Chirp1.

The transmission of each grating was measured with an optical spectrum analyser. From this measurement, we deduced the maximum of the power reflection coefficient R_{max}. The results are reported in the Table 1.

Table 1: Maximum of the power reflection coefficient of the different gratings.

	Unif1	Unif2	Unif3	Step2	Chirp1	Chirp2	Chirp3	Chirp4
R_{max}	1%	50%	95%	71%	66%	7%	22%	23%

The complex reflection coefficient of each grating was measured at least ten times using the LCI system. We then proceeded to the index profile reconstruction using both LP and GLM algorithms. Figure 2 shows the synthesized modulation amplitude of each grating. The profiles obtained with the LP algorithm are plotted with straight lines and those obtained with the GLM algorithm with circles. At first glance, curves are well superimposed (except for the grating Unif3) which means that both methods have almost the same efficiency.

The validity of the reconstruction of modulation amplitude was checked by comparing the profiles we obtained with others given by "Side Diffraction" measurements. Agreement was always good except for the grating Unif3. LP and GLM algorithm failed to achieve a correct synthesis in this case because the grating is highly reflecting (R_{max} = 95%). The result is worse with GLM algorithm even after 30 iterations. This gives an upper limit to the validity of experimental synthesis of FBG using inverse methods.

The sensitivity is very good since we can reconstruct the profile of low reflecting gratings such as Unif1 whose reflection coefficient is 1%. We find in this case a modulation amplitude close to 2.10^{-5}. This is so small that this grating would hardly be detected by conventional method. The same conclusion holds for Step2 : the weakest grating, whose modulation amplitude is close to 2.5 10^{-5}, appears clearly in the synthesized profile. The sensitivity is the same for both algorithms. Indeed, for weak gratings, the limiting factor is the noise in measurements. The sensitivity depends then only on the sensitivity of the measurement device. The method we proposed profits from the high sensitivity of LCI measurements.

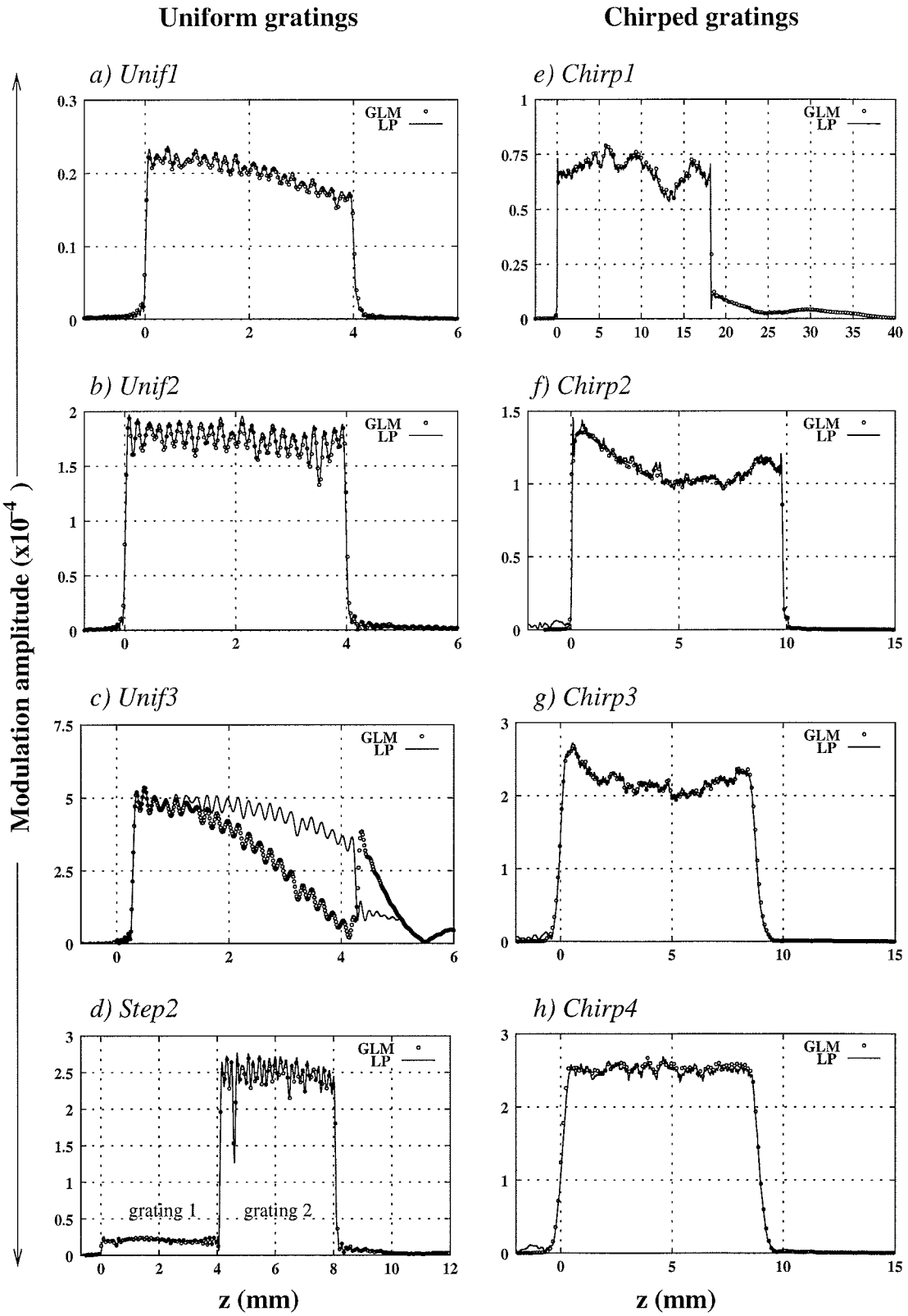

Figure 2: Modulation amplitude of the studied gratings synthesized by LP (straight lines) and GLM (circles).

Each grating was measured ten successive times and each measurement was used to synthesize the grating with both GLM and LP algorithms. An example is given on Figure 3(a) which shows the ten profiles of the grating Unif2 corresponding to successive measurement. The repeatability curve on the same figure corresponds to the maximum, at each point of the grating, of the relative deviation from the mean. For the grating Unif2 and with the GLM algorithm this deviation does not exceed 3.2%. We find similar results for the others gratings and for the LP algorithm. The repeatability of the LP algorithm is a little bit better than that of GLM. Nevertheless, for both algorithms the repeatability is always better than 5%.

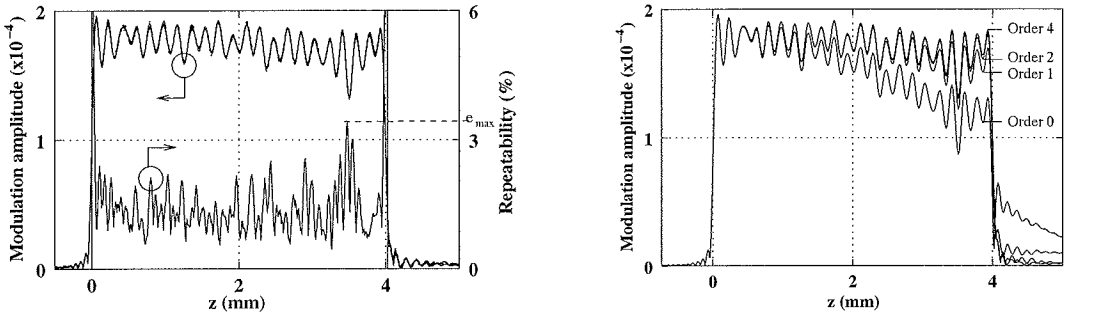

(a) Modulation amplitude (10 profiles) and relative deviation from the mean profile along the grating

(b) Successive profiles given by the GLM algorithm

Figure 3: Modulation amplitude of grating Unif2 synthesized with GLM algorithm : (a) repeatability and (b) convergence.

As far as the modulation amplitude is concerned, the GLM and LP algorithms have the same sensitivity, the same dynamic range and almost the same repeatability. The major difference between them is the duration of the synthesis. The GLM indeed needs several iterations to reach the solution. For example, 4 iterations are needed to synthesize the grating Unif2, see Figure 3(b). As a consequence, this algorithm is very slow compare to the LP algorithm.

4.2 Chirp

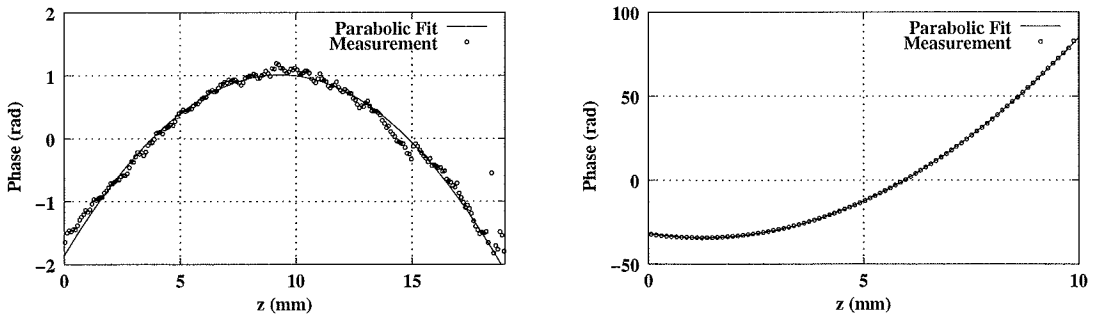

(a) Chirp1

(b) Chirp2

Figure 4: Phases of gratings Chirp1 and Chirp2 synthesized with GLM algorithm. Both curves are fitted with a second order polynomial function.

Figure 4 shows the phases of gratings Chirp1 and Chirp2 synthesized with the GLM algorithm. Similar profiles were obtained for the other gratings and with the LP algorithm. According to eqn. (27), the synthesized phases were fitted by a quadratic function, whose second order coefficient gives the chirp α. Table 2 shows the mean chirps over ten measurements of the different gratings for one direction of propagation. The uncertainties correspond to the half range of the ten measurements.

Table 2: Comparison of the chirps measured with GLM and LP algorithm. All the values are expressed in nm/cm.

	Chirp1	Chirp2	Chirp3	Chirp4
$\mid < \alpha > \mid_{GLM}$	0.030 ± 0.002	1.416 ± 0.002	1.418 ± 0.002	1.427 ± 0.003
$\mid < \alpha > \mid_{LP}$	0.030 ± 0.002	1.428 ± 0.002	1.427 ± 0.003	1.428 ± 0.002

The values of chirp obtained with GLM and LP are in perfect agreement for the gratings Chirp1 and Chirp4, but they differ significantly for the gratings Chirp2 and Chirp3. We are more confident with the LP algorithm for

two reasons. Firstly, the gratings Chirp2 to Chirp4 were written with the same mask, they are then expected to have the same chirp. This is what we obtain with LP whereas in the case of the GLM algorithm, the chirp of the grating Chirp4 is different from the two others. Secondly, the expected value of the chirp of these gratings is 1.5 nm/cm. The results given by LP algorithm are closer to the theoretical values than that of the GLM algorithm.

For both algorithms, the range of measured chirps is of order of 0.005 nm/cm. This gives the lower limit of chirps that can be measured with this method.

5. CONCLUSION

In this paper we have shown that the combination of LCI measurements and inverse scattering algorithms is an efficient method to locally characterise Fibre Bragg Gratings. We studied two algorithms : the Layer Peeling and an iterative solution of the Gel'fand-Levitan-Marchenko coupled equations. Both algorithms give similar results. The LP has a slightly better repeatability of modulation amplitude measurement and a slightly better accuracy in chirp measurements but its major advantage is its speed. It takes a few minutes to synthesize a highly reflecting grating with the GLM, whereas a few seconds are enough with the LP.

Compared to the conventional "Side diffraction", this method presents several advantages due to the measurement process. Firstly, the light scanning the grating propagates inside the fibre where the grating is written. It means that measurement can be performed even if the grating is encapsulated, recoated or embedded in host material. Secondly, this method gives the phase of the grating. This makes possible the detection and characterisation of phase jumps that are inscribed in some kind of gratings. And finally, as the chirp of the grating can be measured, it becomes possible to characterise phenomena that only change the period of the grating such as a gradient of strain or temperature.

REFERENCES

1. M. J. Ablowitz, Lectures on the inverse scattering transform. *Stud. Appl. Math.* (1978), **58**, 17–98.
2. X. Chapeleau, D. Leduc, C. Lupi, R. L. Ny, M. Douay, P. Niay and C. Boisrobert, Experimental synthesis of fiber bragg gratings using optical low coherence reflectometry. *Appl. Phys. Lett.* (2003), **82**, 4227–4229.
3. S. Dyer, K. B. Rochford and A. Rose, Fast and accurate low-coherence interferometric measurements of fiber bragg grating dispersion and reflectance. *Optics Express* (1999), **5**(11), 262–266.
4. R. Feced, M. Zervas and M. Muriel, An efficient inverse scattering algorithm for the design of nonuniform fiber Bragg gratings. *IEEE J. Quantum Electronics* (1999), **35**(8), 1105–1115.
5. P. Giaccari, H. Limberger and R. Salathé, Local coupling coefficient characterization of fiber Bragg gratings. *Optics Lett.* (2003), **28**(8), 598–600.
6. K. Hill, B. Malo, F. Bilodeau and J. Albert, Bragg gratings fabricated in monomode photosensitive optical fiber by UV exposure through a phase mask. *Appl. Phys. Lett.* (1993), **62**(10), 1035–1037.
7. R. Kashyap, *Fiber Bragg gratings. Optics and Photonics*, Academic Press, London, (1999).
8. D. Leduc, X. Chapeleau, C. Lupi, R. Le Ny and C. Boisrobert, Accurate low-coherence interferometric relative group delay and reflectance measurements; characterization of a free space optics multiplexer/demultiplexer. *J. Optics A : Pure Appl. Optics* (2003), **5**, 124–128.
9. E. Peral, J. Capmany and J. Marti, Iterative solution to the Gel'fand-Levitan-Marchenko coupled equations and application to synthesis of fiber gratings. *J. Quantum Electronics* (1996), **32**(12), 2078–2084.
10. L. Poladian, Simple grating synthesis algorithm. *Optics Lett.* (2000), **25**(11), 787–789.
11. E. Robinson, Dynamic predictive deconvolution. *Geophys. Prospecting* (1975), **23**, 779–797.
12. J. Sipe, L. Poladian and C. M. de Sterke, Propagation through nonuniform grating structures. *JOSA A* (1994), **11**(4), 1307–1320.
13. J. Skaar, L. Wang and T. Erdogan, On the synthesis of fiber Bragg gratings by layer peeling. *IEEE J. Quantum Electronics* (2001), **37**(2), 165–173.
14. G. Song, Theory of symmetry in optical filter responses. *JOSA A* (1994), **11**(7), 2027–2037.
15. G. Song and S. Shin, Inverse scattering problem for the coupled-wave equations when the reflection coefficient is a rationnal function. *Proceedings of the IEEE* (1983), **71**(2), 266–268.
16. G. Song and S. Shin, Design of corrugated waveguide filters by the Gel'fand-Levitan-Marchenko inverse-scattering method. *JOSA A* (1985), **2**(11), 1905–1914.
17. A. Yariv, Coupled-mode theory for guided wave optics. *IEEE J. Quantum Electronics* (1973), **QE-9**(9), 919–933.